Journal of Structural Biology **131,** 10–18 (2000)
doi:10.1006/jsbi.2000.4243, available online at http://www.idealibrary.com on IDEAL®

Automated Electron Tomography of the Septal Pore Cap in *Rhizoctonia solani*

Wally H. Müller,*,† Abraham J. Koster,* Bruno M. Humbel,* Ulrike Ziese,* Arie J. Verkleij,* Adriaan C. van Aelst,‡ Theo P. van der Krift,* Roy C. Montijn,§ and Teun Boekhout†

**Department of Molecular Cell Biology, EMSA, Utrecht University, Padualaan 8, 3584 CH Utrecht, The Netherlands; †Yeast Division, Centraalbureau voor Schimmelcultures, Julianalaan 67, 2628 BC Delft, The Netherlands; ‡Department of Plant Cytology and Morphology, Agricultural University of Wageningen, Arboretumlaan 4, 6703 BD Wageningen, The Netherlands; and §Department of Molecular Genetics and Gene Technology, TNO Food and Nutrition Research Institute, Utrechtse weg 48, 3700 AJ Zeist, The Netherlands*

Received November 29, 1999, and in revised form February 2, 2000

Dolipore septa and septal pore caps (SPCs) in filamentous basidiomycetes may play an important role in maintaining the integrity of hyphal cells. We have investigated the ultrastructure of the dolipore septum and the SPC in *Rhizoctonia solani* hyphal cells after high-pressure freezing, freeze substitution, and Spurr embedding. We visualized the SPC with associated cell ultrastructures in three dimensions by automated electron tomography of thick-sectioned cells, followed by 3D tomographic reconstructions. Using these methods we were able to document the passage of mitochondria through the SPC, small tubular membranous structures at the entrance of the septal pore channel, filamentous structures connecting the inner side of the SPC with pore-plugging material, thin filaments anchoring the pore-plugging material with the plasma membrane, small vesicles attached to the plugging material, and tubular endoplasmic reticulum continuous with the base of the SPC. We hypothesize that the SPC, the filamentous structures, the plugging material, and the endoplasmic reticulum act in a coordinated fashion to maintain cellular integrity, intercellular communication, and the transport of solutes and cell organelles in the filamentous fungus *R. solani*. © 2000 Academic Press

***Key Words:* β-1,6-glucan; cryo-scanning electron microscopy; dolipore septum; electron tomography; filamentous structures; freeze substitution; fungus; high-pressure freezing; *Rhizoctonia solani;* septal pore cap; transmission electron microscopy; ZIO staining.**

INTRODUCTION

Septa and septal pore caps (SPCs) play an important role in maintaining cellular homeostasis in filamentous basidiomycetes (Markham, 1995; Müller *et al.*, 1998a). Communication between neighboring hyphal cells occurs through the septal pore channel. As a response to stress or aging, for example, the septal pore channel can be plugged. To understand this blocking mechanism, it is necessary to determine the 3D architecture of the channel, the associated SPCs, and associated cellular ultrastructures. Using electron tomography, cellular structures and arrangements can be studied in 3D with a resolution of 2–10 nm (Koster *et al.*, 1992; Frank, 1995). Examples of structural studies of sections with electron tomography are the 3D visualization of chromosomes (Horowitz *et al.*, 1994) and mitochondria (Perkins *et al.*, 1997).

Despite previous ultrastructural studies of the perforate SPC in basidiomycetes by conventional transmission electron microscopy (e.g., Bracker and Butler, 1964; Casselton *et al.*, 1971; Ellis *et al.*, 1972; Flegler *et al.*, 1976; Girbardt, 1958; Moore, 1985; Müller *et al.*, 1998a; Orlovich and Ashford, 1994; Wilsenach and Kessel, 1965), a full understanding of the function of these structures has been lacking. There are two main reasons for this. First, conventional preparative procedures for electron microscopy typically cause dramatic changes in the ultrastructure of fungal cells. Second, in plastic sections—even in cryo-fixed and freeze-substituted fungal cells—large cellular structures can hide smaller ones, which limits the resolution of those methods.

To avoid these shortcomings we studied the 3D ultrastructure of the SPC and associated cellular structures of the plant pathogenic fungus *Rhizoctonia solani* by use of high-pressure freezing (HPF) (Müller and Moore, 1984; Studer *et al.*, 1995), freeze substitution (FS) (Howard and Aist, 1979; Müller *et al.*, 1980), and electron tomography (ET) (Koster *et*

1047-8477/00 $35.00

al., 1997). Compared to other preparations, the combined use of HPF–FS–ET allowed for documentation of SPC structure and associated plugging elements with unprecedented detail. Understanding the channel plugging mechanism could reveal alternative methods for inhibiting growth of this plant pathogenic basidomycete.

MATERIALS AND METHODS

Organism and culture. Strain CBS 346.84 of *R. solani* was maintained on YMA (0.3% yeast extract–0.3% malt extract–0.5% peptone–1% dextrose–2% agar) medium as described previously (Müller *et al.*, 1998a).

Ambient temperature and cryo-scanning electron microscopy (SEM). To visualize the internal organization of *R. solani* hyphae at ambient temperature, we used the preparation method of Müller *et al.* (1998b). For cryo-SEM, 5 × 8 mm rectangles were cut with a razor blade from 3-day-old cultures. After chemical fixation with 3% (v/v) glutaraldehyde in 50 mM sodium cacodylate buffer (SCB), pH 7.4, and washing with SCB, the fungal samples were infiltrated with 2.1 M sucrose in SCB at room temperature for 16 h, and, after being mounted in tissue-freezing medium on a transfer holder of the Oxford CT 1500 HF cryo-SEM device (Oxford, UK), frozen in liquid nitrogen. Once inside the CT 1500HF preparation chamber, the chemically pretreated and cryo-fixed samples were loaded, fractured at a temperature of −100°C, held at −95°C for 5 min, and subsequently coated with platinum by magnetron sputtering for 1 min at 5×10^{-6} bar, corresponding to a thickness of ca. 5 nm. The coated fungal fragments were examined in a field emission cryo-scanning electron microscope (JSM 6300F, Jeol) at 5 kV and a working distance of 11 mm.

Transmission electron microscopy (TEM). To detect the calcium affinity sites in the endoplasmic reticulum connected to the SPC, hyphae of *R. solani* were immersed in a solution of zinc–iodine–osmium tetroxide (ZIO) as described by Hawes (1991) and further prepared for TEM as described by Müller *et al.* (1998b).

Cryo-fixation and freeze substitution. High-pressure freezing, freeze substitution, and subsequent processing for TEM were performed as described by Müller *et al.* (1998a).

Immunogold labeling. Spurr (1969) sections of *R. solani* hyphae were incubated with affinity-purified polyclonal antibodies (1:300) recognizing β-1,6-glucan (Montijn *et al.*, 1994). The glucan–antibody complexes were visualized with goat anti-rabbit antibodies (1:10) conjugated with 10-nm gold particles (Aurion, The Netherlands).

Electron tomography. High-pressure frozen, freeze-substituted, and Spurr embedded hyphae of *R. solani* were thick sectioned (250 nm) and mounted on a microscope grid with an EM perfect loop (Electron Microscopy Sciences, Fort Washington, PA). The grids with the sections were subsequently placed on a droplet of double-distilled water (dH_2O) and a 50-μL droplet of 0.02% aqueous poly-L-lysine for 10 min, thoroughly rinsed with dH_2O, and dried for 15 min at 65°C. The grids with sections were gently placed on 50-μL droplets of 1:2 diluted 13-nm gold solution (sodium citrate solution by Turkevich *et al.*, 1951) for 60 s and thereafter thoroughly rinsed with dH_2O and dried for 15 min at 65°C. After being dried, the grids with sections facing up were carbon-coated.

For viewing, sample grids were mounted on a Gatan high-tilt cryo-transfer holder (Gatan, Pleasanton, CA) operated at room temperature. After preirradiation to stabilize the sections (Braunfeld *et al.*, 1994; Luther *et al.*, 1988), tilt series were collected at low and high magnifications of 5000 and 15 000×, respectively (Koster *et al.*, 1997). The angular tilt range covered −73° to +69° with a 1° tilt increment. Exposure time per image was 1 s. The tilt series was taken with a Philips CM200 FEG-TEM (FEI/Philips, Eindhoven, The Netherlands) operating at 200 kV. The defocus was 3.4 μm, corresponding to the first zero in the contrast transfer function of the EM at 2.9-nm periodicity. The images were recorded with a cooled slow-scan CCD camera, having 1024 × 1024 pixels of 24 μm. The pixel size at the plane of the sample was 2.51 nm (magnification 5000×) and 0.86 nm (magnification 15 000×), respectively. The TEM and CCD camera were controlled by a TVIPS computer system (TVIPS GmbH, Gauting, Germany), using a program for automatic tomographic data collection (Dierksen *et al.*, 1992). A period of 4 h was required to document a single tilt series of 150 projections. Image processing, i.e., alignment of tilt series and 3D reconstruction, was performed on a Unix workstation (Silicon Graphics dual-processor Octane) equipped with EM System (Hegerl, 1996), IVE (Fung *et al.*, 1996), and Imod (Kremer *et al.*, 1996) software, using the 13-nm gold beads as "landmarks" (Frank, 1992).

RESULTS

Scanning Electron Microscopy

Ambient temperature SEM clearly revealed the morphology of the perforate SPC in transversally fractured hyphal cells of *R. solani* (Fig. 1a). The SPCs measured about 1600–2000 nm in width and contained three to five circular to ellipsoid perforations of about 800 nm in diameter. Mitochondria were observed within SPC perforations, presumably in transit. The SPCs covered the dolipore septum. A plug blocked the entrance of the septal pore channel. Between the rim of the entrance of the septal pore channel and the SPC, remnants of filamentous structures were observed. Furthermore, the SPC was covered with some fine fibrillar material. In cryo-SEM the perforate SPCs could only rarely be seen in longitudinally fractured *R. solani* hyphae; they measured about 1600–1800 nm in diameter (Fig. 1b).

Transmission Electron Microscopy

In ZIO-stained hyphal sections of *R. solani* the lumen of the endoplasmic reticulum (ER) appeared electron-dense. Only the outer and inner membranes of the SPC were ZIO-stained, while the SPC matrix remained unstained (Fig. 2a). Mitochondria were observed inside the perforations of the SPC and in the septal pore channel. The dolipore septum showed a shrunken appearance. The connection of the ER with the base of the SPC could not be properly visualized.

In sections of cryo-fixed and freeze-substituted hyphae of *R. solani* filamentous structures were present in the area between the SPC and the plugging material (Fig. 2b). In near-median sections these filamentous structures resembled the spokes in an umbrella. When the pore-plugging material

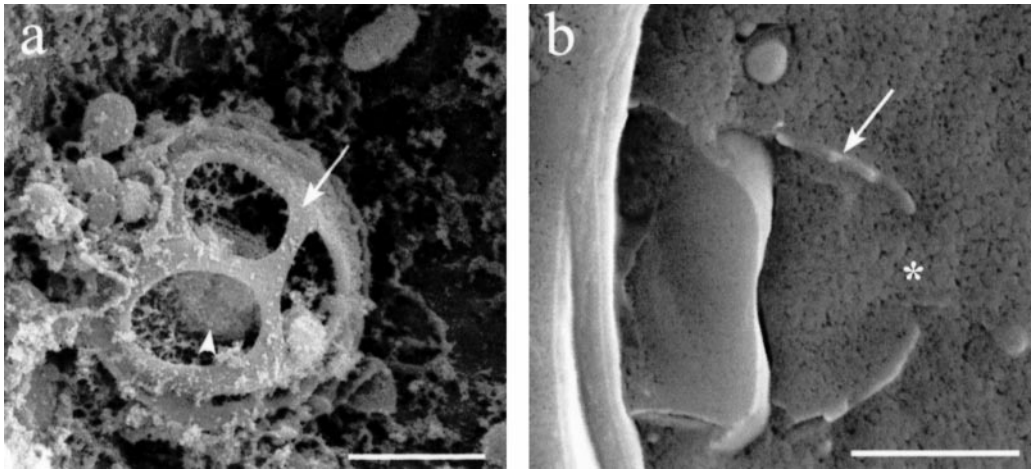

FIG. 1. Scanning electron microscopy of the perforate septal pore cap of *Rhizoctonia solani*. (a) Ambient temperature SEM shows the SPC covering the entrance of the septal pore channel. The perforate SPC (arrow) has three visible holes, allowing the passage of organelles. Remnants of filamentous material are present on the outer surface of the SPC and between the inner side of the SPC and the dolipore (arrowhead). (b) Cryo-SEM shows only in longitudinally fractured hyphal cells the typical morphology of the perforate SPC. Asterisk indicates one of the holes of the SPC. Bars, 1 μm.

had the appearance of a cork-shaped structure, the entrance of the dolipore septum was completely blocked. In addition, the cork-like pore-plugging material appeared to be electron translucent at its core. Moreover, those parts of the SPC connected with the filamentous structures had a matrix with a lower electron density or this matrix was even not present compared to the matrix of the unconnected cap parts (Fig. 2c).

β-1,6-Glucan was immunocytochemically detected predominately in the septal swellings and smaller amounts were found in the septal plate (Figs. 2b and 2c). No cytosolic β-1,6-glucan was detected.

Electron Tomography

Three-dimensional reconstructions of thick sections of cryo-fixed and freeze-substituted hyphae of *R. solani* showed the presence of mitochondria

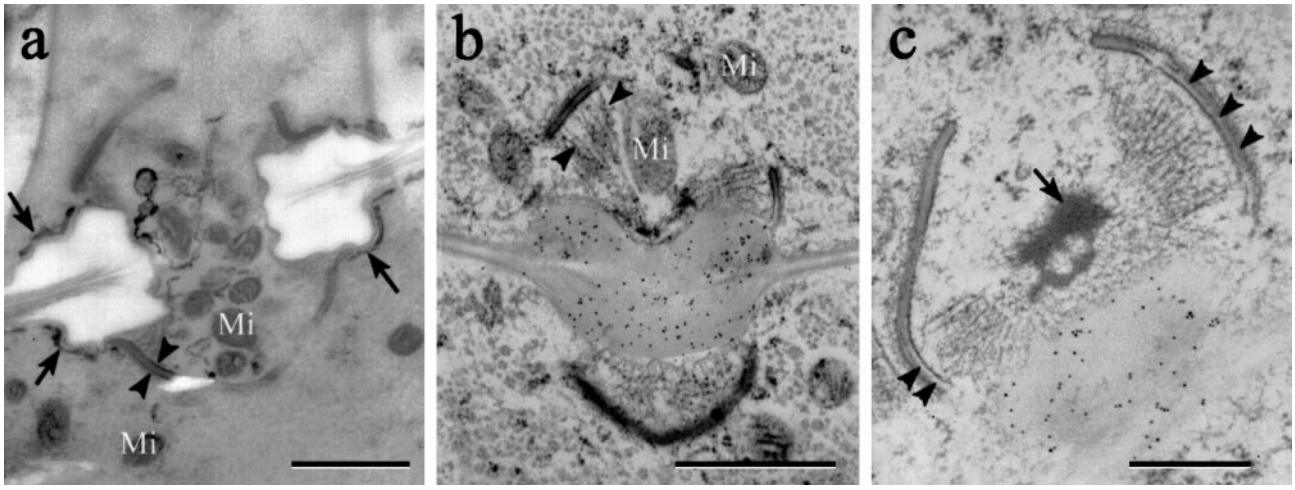

FIG. 2. Transmission electron microscopy of the perforate septal pore cap of *Rhizoctonia solani*. (a) Chemical fixation and zinc–iodine–osmium tetroxide staining of the dolipore septum and the SPC show that the endoplasmic reticulum is stained (arrows), as are the outer and inner membranes of the SPC (arrowheads), while the SPC matrix is unstained. (b and c) Cryo-fixation and freeze substitution of the dolipore septum and the SPC. Between the inner side of SPC and the pore-plugging material a network of filamentous structures (arrowheads) is present, which cannot be observed in chemically fixed cells as shown in a. (c) A near-median section of the dolipore and the SPC. Note that the inner side of the plug (arrow) is translucent. Those parts of the SPC that are connected with the filamentous structures show a less electron-dense SPC matrix (arrowheads) than the remainder of SPC matrix. Gold labels in b and c show the location of β-1,6-glucan in the dolipore. Mi, mitochondrion. Bars (a, b) 1 μm; (c) 500 nm.

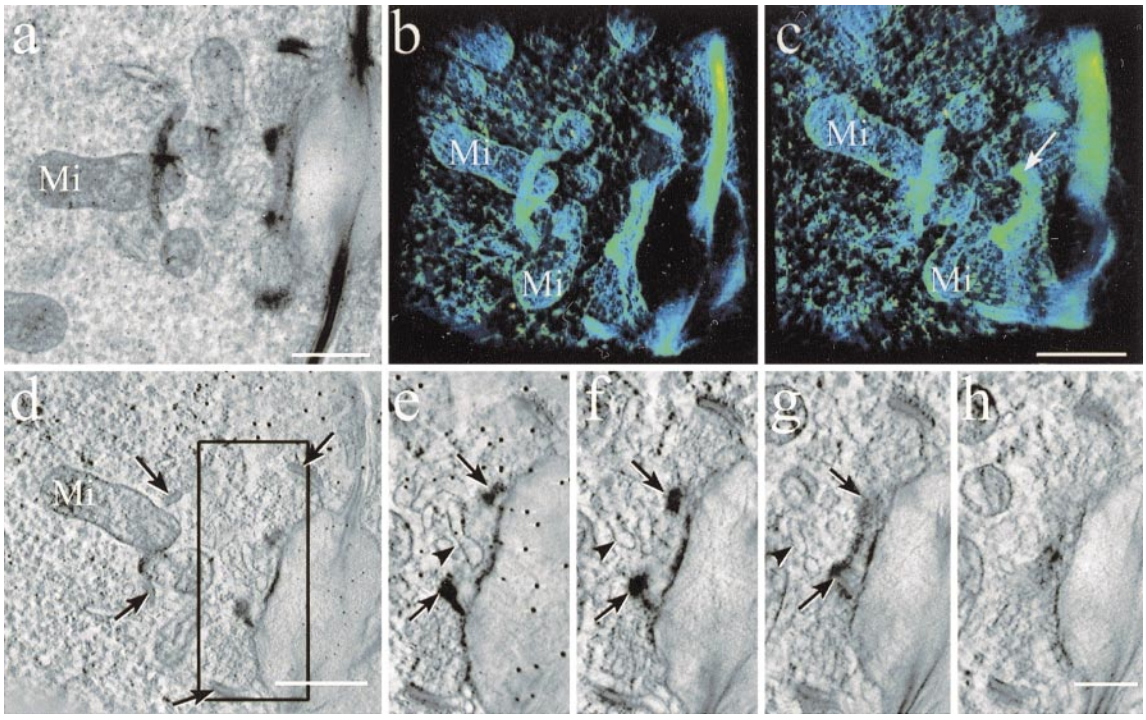

FIG. 3. Automated electron microscopy showing two ways of visualizing hyphal cell ultrastructures by volume rendering and slices of a tomogram. (a) Original 220-nm-thick section of cryo-fixed and freeze-substituted dolipore septum, perforate septal pore cap of *Rhizoctonia solani,* and associated cellular structures. (b and c) Volume rendering of the dolipore septum and the SPC. Mitochondria (Mi) are passing the SPC. In c, by tilting b, a part of the ring-like structure of the pore-plugging material (arrow) is better observed than in a and b. (d) A 15-nm slice of a tomogram shows clearly the passage of a mitochondrion (Mi) through the SPC (arrow). (e and f) A gallery of 15-nm slices of the marked area in d. At the entrance of the opened septal pore channel tubular membranous structures are present (arrowheads). In cross-sectioned ring-like pore-plugging material, the plugging material manifests as two electron-dense globular, stalk-like structures attached to the septal swellings (arrows). The gold particles show a dotted pattern in a–e and function as landmarks for the image processing in AET. Bars (a, c, d) 500 nm; (h) 250 nm.

within the perforations of the SPC as well as in the cytoplasmic space between the SPC and the dolipore, together with other cellular structures. The unblocked septal pore channel was lined by a ring of electron-dense material (Fig. 3). Furthermore, small globose–tubular membranous structures of about 80 nm were observed near the entrance of the septal pore channel (Fig. 3). Tubular endoplasmic reticulum was continuous with the base of the SPC (Fig. 4).

Filamentous structures of ca. 10 nm in thickness connected the inner side of the SPC with the pore-plugging material and showed a fork-like connection with the inner membrane of the SPC (Fig. 4). Moreover, such filamentous structures were found in between fine connections (Fig. 5). Small vesicles of about 45 nm in diameter were attached to the plugging material (Fig. 6). When the entrance of the septal pore channel was not closed, the pore-plugging material was found to be less electron-dense at the outer side, giving it a spongy appearance (Fig. 6). Approximately 10-nm-thick filamentous structures connected the pore-plugging material with the plasma membrane at the septal swelling (Fig. 7).

DISCUSSION

The perforate SPC of the plant pathogenic fungus *R. solani* has been studied extensively by use of conventional electron microscopy (e.g., Bracker and Butler, 1963; Butler and Bracker, 1970; Lisker *et al.*, 1975; Müller *et al.*, 1998b; Setliff *et al.*, 1972). The electron microscopic results of studies on SPCs were the basis for morphological studies on septal occlusion in filamentous fungi (Markham, 1994) or for investigation on basidiomycete phylogeny (McLaughlin *et al.*, 1995a,b). By combining different preparative methods for electron microscopy we were able to resolve more ultrastructural details and to obtain new insights in the architecture of the SPC of *R. solani*. We observed a filamentous network that connected to the inner side of the SPC with the pore-plugging material. By combining high-pressure freezing, freeze substitution, and automated elec-

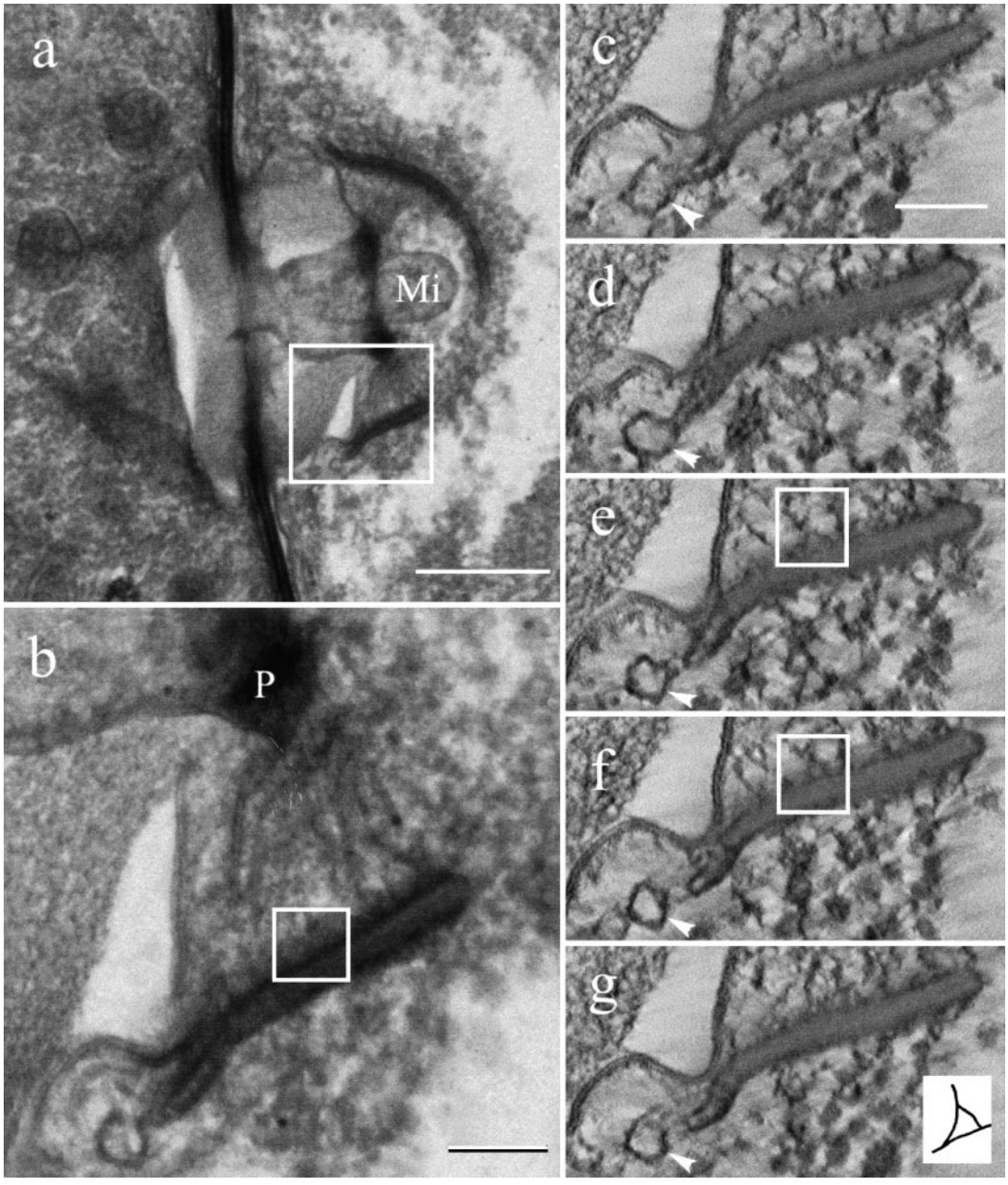

FIG. 4. Automated electron microscopy showing the connection of filamentous structures at the inner side of the septal pore cap of *Rhizoctonia solani*. (a and b) Original 220-nm-thick section of cryo-fixed and freeze-substituted dolipore septum, perforate septal pore cap, and associated cellular structures. In a, a mitochondrion (Mi) is in the entrance of the septal pore channel. (b) A higher magnification view of the marked area in a. (c–g) A gallery of 3.4-nm slices of a tomogram of the area in b. Tubular endoplasmic reticulum is continuous with the base of the SPC (arrowheads). In e and f the fork-like connections with the inner side of the SPC are marked by a white rectangle. Inset in g shows a schematic representation of the fork-like connection. Bar (a) 500 nm; (b and c) 100 nm.

tron tomography, we demonstrate that these filamentous structures of about 10 nm in thickness are attached to the inner membrane of the SPC (Fig. 4). Filaments also connected the pore-plugging material with the septal swelling in opened or closed septal pore channels (Fig. 7). We speculate that these filamentous structures might play a crucial role in plugging the entrance of the septal pore channel.

While the application of the morphologically highly reliable cryo-techniques is a prerequisite for the fine analysis of the organization of the SPC, its

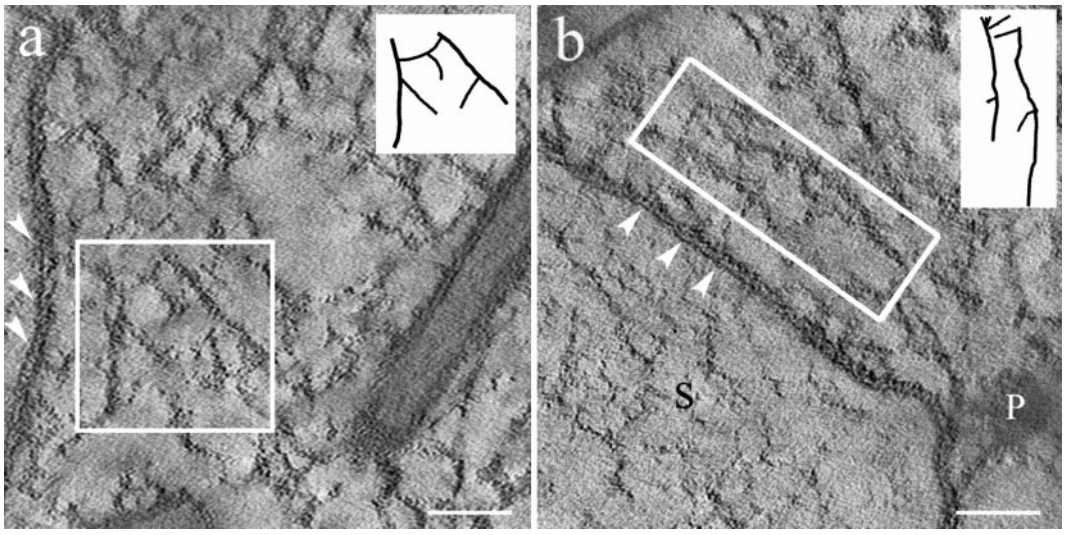

FIG. 5. Two 3.4-nm slices of a tomogram of parts of the filamentous network in between the pore-plugging material (P) and the inner side of the perforate septal pore cap of *Rhizoctonia solani*. Fine connections are present in between the filaments. Inset shows a schematic representation of the marked area. S, septal swelling; arrowheads indicate the plasma membrane. Bars, 100 nm.

use in combination with the less reliable conventional methods may complete the overall view. Chemically fixed hyphae of *R. solani* revealed the existence of the SPC (Bracker and Butler, 1964; Figs. 1 and 2a); however, the connection between the SPC and the plug could not be observed. Cryo-fixation and freeze substitution are more favorable for ultrastructural preservation. HPF was the method of choice for cryo-fixation of hyphae of *R. solani* to avoid ice crystal damage in thick samples of colonies of this fungus. HPF and FS resulted in an improved preservation of the SPC and its associated cellular structures. Filamentous structures in between the SPC and the dolipore have been observed in thin sections of cryo-fixed and freeze-substituted hyphae of *Pisolithus arhizus* (Orlovich and Ashford, 1994) and of *Schizophyllum commune* (Müller *et al.*, 1998a). The connections between the SPC and the plug in *R. solani* observed in this communication (Figs. 2b and 2c) resemble those filamentous structures reported previously. *R. solani,* however, has many more filaments than *P. arhizus* and *S. commune.*

Compared to thin sectioning, the automated electron tomographic reconstructions of thick sections show more ultrastructural details. The merits of this technique are as follows: (1) no serial sections are needed, (2) filamentous structures can easily be followed in the thick section, (3) hidden structures can be revealed, (4) the ultrastructure of interest can be easily oriented, and (5) there is possibly less ultrastructural damage caused by cutting sections. There is evidence that the cutting process damages the ultrastructure on the section surface. Thus the thicker the section, the more continuous, well-preserved structural detail might be revealed. The calculated sections from the 3D volume circumvent this physical cutting problem. The reconstructions (Figs. 3–7) of thick sections of high-pressure frozen and freeze-substituted *R. solani* hyphae revealed how the filaments are attached to the inner membrane of the SPC (Fig. 4) and how filaments connect the pore-plugging material with the dolipore (Fig. 6 and 7). Further studies are needed to elucidate whether the fine connections in between the filaments are real or are deposits of small ice crystals formed by insufficient cryo-fixation (Fig. 5).

In young hyphal cells, the plugging material that blocks the entrance of the septal pore channel appears to be reversible, while in mature hyphal cells the plug may be more permanent (Bracker, 1992). In response to stress, plugs block the transport of cellular constituents from one cell to another. In filamentous fungi, the plug might originate from a coagulation of cytoplasmic components or organelles (Aylmore *et al.*, 1984), from the matrix material of the SPC (Markham, 1994), or from both (Müller *et al.*, 1998a). We suggest that the matrix of the SPC in *R. solani* might be transported by the filamentous structures to reach the entrance of the septal pore channel. The nature of the filamentous structures is yet unclear. In this way the SPC has a repository function, as postulated earlier by Markham (1994); hence the SPC matrix becomes electron translucent as demonstrated (Fig. 2c). In the early stage of plug formation a ring of electron-dense material is depos-

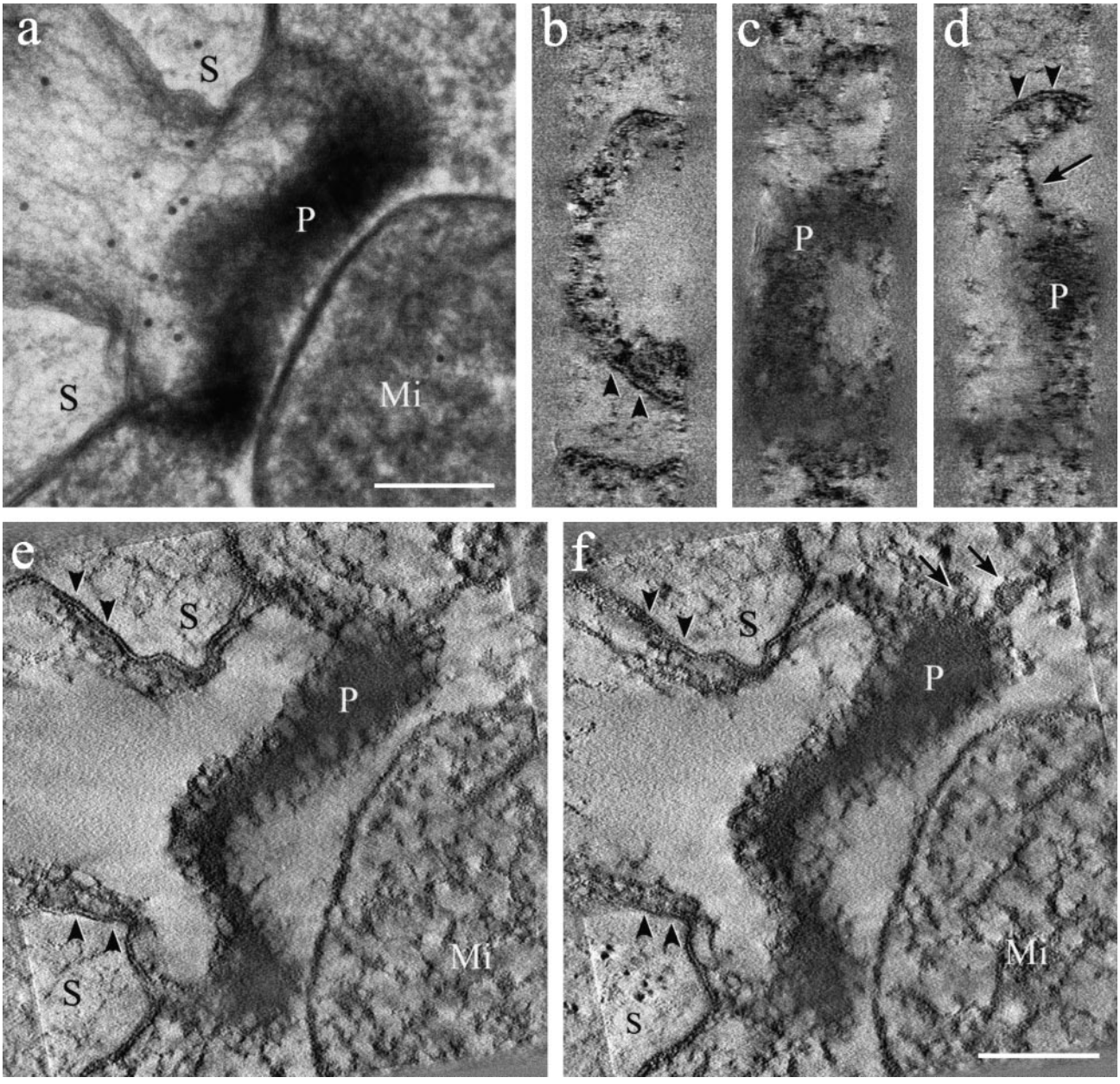

FIG. 6. The ring-like plugging material at the entrance of the septal pore channel of *Rhizoctonia solani* after automated electron microscopy. (a) Original 220-nm-thick section of cryo-fixed and freeze-substituted part of the pore-plugging material (P), which is attached to the septal swelling (S). The gold particles, indicated as black dots, function as landmarks for the image processing after AET. (b–d) Perpendicular views of a with a part of the septal pore channel (b), a part of the ring-like pore-plugging material (c), and electron-dense material (d) bridging the pore-plugging material with the plasma membrane (arrowheads) at the septal swelling. (e and f) Two 1.7-nm slices of a tomogram of the pore-plugging material, showing inside the plugging material an electron-dense compact structure, while the outer side appears less electron-dense and shows a spongy appearance. In f small vesicles are attached to the pore-plugging material (arrows). Arrowheads indicate the plasma membrane; S, septal swelling. Bars, 200 nm.

ited at the rim of the entrance of the septal pore channel. In a perpendicular section, this ring is resolved as two aggregates of high electron density on top of the rim (Fig. 3). The flow of plugging material continues in a later stage, finally resulting in a plug that closes the entrance of the septal pore channel (Fig. 2). It is possible that next to the matrix of the SPC, small vesicles are also involved in depositing pore-plugging material (Fig. 6). The plugging material may be anchored to the rim of the septal pore channel by filaments (Fig. 7). Disassembly of the plugging material may be performed by enzymes in

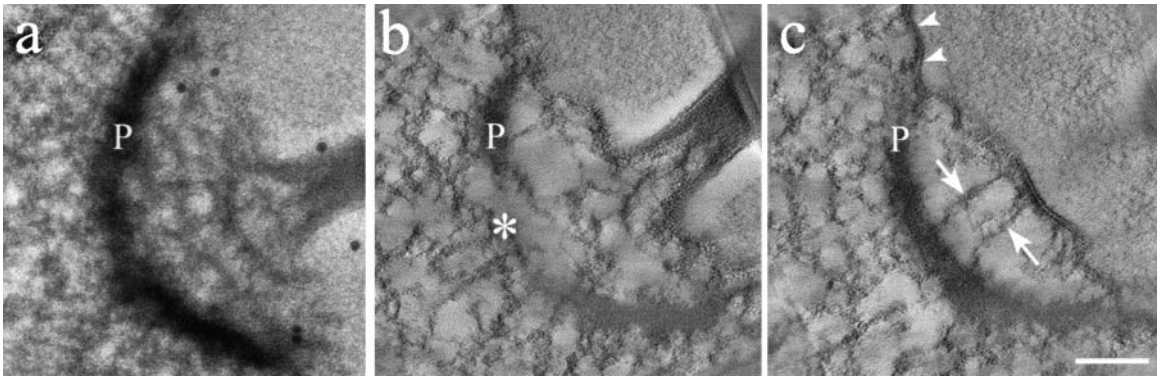

FIG. 7. Automated electron microscopy showing the connection of the pore-plugging material (P) with the plasma membrane (arrowheads) at the spot of the septal pore channel of *Rhizoctonia solani.* (a) Original 220-nm-thick section of cryo-fixed and freeze-substituted dolipore septum and pore-plugging material. The entrance of septal pore channel is covered by dome-shaped plugging material, suggesting that the entrance is blocked. The black dots are gold particles that function as landmarks for the image processing after AET. (b and c) Two 2.5-nm slices of a tomogram of a. (b) Opposite the entrance of the septal pore channel the plugging material is not closed (asterisk). (c) Filaments (arrows) connect the pore-plugging material with the plasma membrane (arrowheads). Bar, 100 nm.

the septal pore channel or in the cytoplasm near the plugging material. If this model of plug formation is valid, one must postulate a signaling system to coordinate the formation and disassembling of the plug processes. This signaling system would start with an initial cytoplasmic signal—indicating that the entrance of the septal pore channel needs to be plugged—to the SPC, endoplasmic reticulum, and filamentous network connecting the SPC and would finally result in the formation of a plug.

To better understand the functioning of the SPC in basidiomycete fungi, its biochemical architecture, its connection with other cellular structures, and its possible role in signal transduction must be known. Based on the results of our study, we propose that the perforate SPC of *R. solani* is connected at its base with tubular endoplasmic reticulum. It is yet unclear how and when the SPC is formed. Several studies have shown that the SPC is present after completion of dolipore septum development (Butler and Bracker, 1970; Guo *et al.*, 1996). The number of perforations of the SPC of *R. solani* varies between 3 and 5. It is still unclear how these perforations are formed, how long they exist in the cap, and whether they are fixed in the cap or are dynamic. The cap consists of an outer membrane and an inner membrane, confining a matrix. The nature of the matrix is not yet known, but it is likely one of the main constituents of the plugging material. Against both membranes of the cap, an electron-dense layer is present, which is thicker at the outer membrane than at the inner membrane. The plugging material in opened and closed septal pore channels is anchored to the rim of the entrance of the septal pore channel by filaments. When the plug blocks the entrance of the septal pore channel, intercellular communication and transport of cellular constituents will be inhibited. The filamentous structures, connecting the inner side of the SPC with the plugging material at the entrance of the septal pore channel, are likely to be involved in the transport of plugging material and therefore may play a key role in plug formation.

The authors thank Dr. R. J. Howard (DuPont Central Research and Development, Wilmington, DE) for help with the manuscript; Prof. Dr. W. Gams and Dr. D. van der Mei (Centraalbureau voor Schimmelcultures, Baarn, NL) for critically reading the manuscript; and Wil van Veenendaal, Ronald Leito, Piet Brouwer, and Frits Kindt (Utrecht University, Utrecht, The Netherlands) for the preparation of the photographs. This work is based on a cooperative project between the Centraalbureau voor Schimmelcultures and Utrecht University. The research of Dr. A. J. Koster has been made possible by a fellowship of the Royal Netherlands Academy of Arts and Sciences.

REFERENCES

Aylmore, R. C., Wakley, G. E., and Todd, N. K. (1984) Septal sealing in the basiodiomycete *Coriolus versicolor, J. Gen. Microbiol.* **130,** 2975–1982.

Bracker, C. E. (1992) Intercellular cytoplasmic connection in fungi, *in* Second International Workshop on Basic and Applied Research in Plasmodesmatal Biology, pp. 89–93, Oosterbeek, The Netherlands.

Bracker, C. E., and Butler, E. E. (1963) The ultrastructure and development of septa in hyphae of *Rhizoctonia solani, Mycologia* **55,** 35–58.

Bracker, C. E., and Butler, E. E. (1964) Function of the septal pore apparatus in *Rhizoctonia solani* during protoplasmic streaming, *J. Cell Biol.* **21,** 152–157.

Braunfeld, M. B., Koster, A. J., Sedat, J. W., and Agard, D. A. (1994) Cryo automated electron tomography: Towards high-resolution reconstructions of plastic-embedded structures, *J. Microsc.* **174,** 75–84.

Butler, E. E., and Bracker, C. E. (1970) Morphology and cytology of *Rhizoctonia solani, in* Parmeter, J. R., Jr. (Ed.), *Rhizoctonia,*

Biology and Pathology, pp. 32–50, Univ. of California Press, Berkeley, CA.

Casselton, L. A., Lewis, D., and Marchant, R. (1971) Septal structure and mating behaviour of common A diploid strains of *Coprinus lagopus*, *J. Gen. Microbiol.* **66,** 273–278.

Dierksen, K., Typke, D., Hegerl, R., Koster, A. J., and Baumeister, W. (1992) Towards automatic electron tomography, *Ultramicroscopy* **40,** 71–87.

Ellis, T. T., Rogers, M. A., and Mims, C. W. (1972) The fine structure of the septal pore cap in *Coprinus stercorarius*, *Mycologia* **64,** 681–688.

Flegler, S. L., Hooper, G. R., and Fields, W. G. (1976) Ultrastructural and cytochemical changes in the basidiomycete dolipore septum associated with fruiting, *Can. J. Bot.* **54,** 2243–2253.

Frank, J. (1995) Approaches to large-scale structures, *Curr. Opin. Struct. Biol.* **5,** 194–201.

Fung, J. C., Liu, W., de Ruiter, W. J., Chen, H., Abbey, C. K., Sedat, J. W., and Agard, D. A. (1996) Toward fully automated high-resolution electron tomography, *J. Struct. Biol.* **116,** 181–189.

Girbardt, M. (1958) Über die Substruktur von *Polystictus versicolor* L, *Arch. Mikrobiol.* **28,** 255–269.

Guo, S., Xu, J., and Xiao, P. (1996) Studies on the septal ultrastructure of *Armilaria mellea* [*Chung Kuo I Hsueh Ko Hsueh Yuan Hsueh Pao*], *Acta Acad. Med. Sinicae* **18,** 363–369.

Hawes, C. R. (1991) Stereo-electron microscopy, *in* Hall, J. L., and Hawes, C. R. (Eds.), Electron Microscopy of Plant Cells, pp. 67–84, Academic Press, London.

Hegerl, R. (1996) The EM program package: A platform for image processing in biological electron microscopy, *J. Struct. Biol.* **116,** 30–34.

Horowitz, R. A., Agard, D. A., Sedat, J. W., and Woodcock, C. L. (1994) The three-dimensional architecture of chromatin in situ: Electron tomography reveals fibers composed of continuously variable zig-zag nucleosomal ribbon, *J. Cell Biol.* **125,** 1–10.

Howard, R. J., and Aist, J. R. (1979) Hyphal tip cell ultrastructure of the fungus *Fusarium:* Improved preservation by freeze-substitution, *J. Ultrastruct. Res.* **66,** 224–234.

Koster, A. J., Chen, H., Sedat, J. W., and Agard, D. A. (1992) Automated microscopy for electron tomography, *Ultramicroscopy* **46,** 207–227.

Koster, A. J., Grimm, R., Typke, D., Hegerl, R., Stoschek, A., Walz, J., and Baumeister, W. (1997) Perspectives of molecular and cellular electron tomography, *J. Struct. Biol.* **120,** 276–308.

Kremer, J. R., Mastronarde, D. N., and McIntosh, J. R. (1996) Computer visualization of three-dimensional image data using IMOD, *J. Struct. Biol.* **116,** 71–76.

Lisker, N., Katan, J., and Henis, Y. (1975) Scanning electron microscopy of the septal pore apparatus of *Rhizoctonia solani*, *Can. J. Bot.* **53,** 1801–1804.

Luther, P. K., Lawrence, M. C., and Crowther, R. A. (1988) A method for monitoring the collapse of plastic sections as a function of electron dose, *Ultramicroscopy* **24,** 7–18.

Markham, P. (1994) Occlusions of septal pores in filamentous fungi, *Mycol. Res.* **98,** 1089–1106.

Markham, P. (1995) Organelles of filamentous fungi, *in* Gow, N. A. R., and Gadd, G. M. (Eds.), The Growing Fungus, pp. 75–98, Chapman and Hall, London.

McLaughlin, D. J., Berres, M. E., and Szabo, L. J. (1995a) Molecules and morphology in basidiomycete phylogeny, *Can. J. Bot.* **73,** S684–S692.

McLaughlin, D. J., Frieders, E. M., and Lü, H. (1995b) A microscopist's view of heterobasidiomycete phylogeny, *Stud. Mycol.* **38,** 91–110.

Montijn, R. C., Van Rinsum, J., Van Schagen, F. A., and Klis, F. M. (1994) Glucomannoproteins in the cell wall of *Saccharomyces cerevisiae* contain a novel type of carbohydrate side chain, *J. Biol. Chem.* **269,** 19338–19342.

Moore, R. T. (1985) The challenge of the dolipore/parenthesome septum, *in* Moore, D., Casselton, L. A., Wood, D. A., and Frankland, J. C. (Eds.), Developmental Biology of Higher Fungi, pp. 175–212, Cambridge Univ. Press, Cambridge.

Müller, M., Marti, T., and Kriz, S. (1980) Improved structural preservation by freeze substitution, *in* Brederoo, P., and De Priester, W. (Eds.), Electron Microscopy, pp. 720–721, North Holland, Amsterdam.

Müller, M., and Moore, H. (1984) Cryofixation of thick specimens by high-pressure freezing, *in* Revel, J. P., Barnard, T., and Haggings, G. H. (Eds.), Science of Biological Specimen Preparation, pp. 131–138, SEM Inc., AMF O'Hare, Chicago.

Müller, W. H., Montijn, R. C., Humbel, B. M., Van Aelst, A. C., Boon, E. J. M. C., Van der Krift, T. P., and Boekhout, T. (1998a) Structural differences between two types of basidiomycete septal pore caps, *Microbiology* **144,** 1721–1730.

Müller, W. H., Stalpers, J. A., Van Aelst, A. C., Van der Krift, T. P., and Boekhout, T. (1998b) Field emission gun-scanning electron microscopy of septal pore caps of selected species in the *Rhizoctonia* s.l. complex, *Mycologia* **90,** 170–179.

Orlovich, D. A., and Ashford, A. E. (1994) Structure and development of the dolipore septum in *Pisolithus tinctorius*, *Protoplasma* **178,** 66–80.

Perkins, G., Renken, C., Martone, M. E., Young, S. J., Ellisman, M., and Frey, T. (1997) Electron tomography of neuronal mitochondria: Three-dimensional structure and organization of cristae and membrane contacts, *J. Struct. Biol.* **119,** 260–272.

Setliff, E. C., MacDonald, W. L., and Patton, R. F. (1972) Fine structure of the septal pore apparatus in *Polyporus tomentosus*, *Poria latemarginata*, and *Rhizoctonia solani*, *Can. J. Bot.* **50,** 2559–2563.

Spurr, A. R. (1969) A low-viscosity epoxy resin embedding medium for electron microscopy, *J. Ultrastruct. Res.* **26,** 31–43.

Studer, D., Michel, M., Wohlwend, M., Hunziker, E. B., and Buschmann, M. D. (1995) Vitrification of articular cartilage by high-pressure freezing, *J. Microsc.* **179,** 321–332.

Turkevich, J., Stevenson, P. C., and Hillier, J. (1951) A study of the nucleation and growth processes in the synthesis of colloidal gold, *Discuss. Farad. Soc.* **11,** 55–75.

Wilsenach, R., and Kessel, M. (1965) On the function and the structure of the septal pore of *Polyporus rugulosus*, *J. Gen. Microbiol.* **40,** 397–400.